American Mineralogist, Volume 72, pages 537–550, 1987

Muscovite dehydroxylation: High-temperature studies

STEPHEN GUGGENHEIM, YU-HWA CHANG, A. F. KOSTER VAN GROOS
Department of Geological Sciences, University of Illinois at Chicago, Chicago, Illinois 60680, U.S.A.

ABSTRACT

Unit-cell dimensions of muscovite-$2M_1$ from the Diamond mine, South Dakota, were determined to 1000°C, single-crystal X-ray structural refinements were made at 20°C and 300°C, and additional structural refinements at 20, 525, and 650°C were made on similar material from Panasqueira, Portugal. Single-crystal data showed linear expansivity of the metric dimensions to about 850°C followed by a phase change to muscovite dehydroxylate with increases in the *b* and *c* parameters and a decrease in *a* near 850°C. The mean atomic distances of the K polyhedron increased more rapidly than those for the other polyhedra as temperature increased. The result shows that (1) the K–O(2) bond is longer than K–O(1) and K–O(3) at each temperature and (2) the K–O(2) bond distance [2.867(3) Å at 20°C] expands with temperature more rapidly [with a mean thermal-expansion coefficient (MTEC) of 5.4] than the other two interlayer bonds [K–O(1): 2.832(3) Å at 20°C, MTEC = 4.7; K–O(3): 2.844(3) Å at 20°C, MTEC = 4.5]. It is concluded that the proton position weakens (lengthens) the K–O(2) bond relative to K–O(1) and K–O(3) and that a preferred path for dehydroxylation results. Misfit between the tetrahedral and octahedral sheets is not a factor in thermal decomposition, since the tetrahedral rotation angle is about 8.5° at 850°C.

Thermal analysis (TGA, DTG) indicated a very broad dehydration peak, interpreted as two overlapping and poorly resolved dehydration peaks at apparently 550 and 750°C on the basis of comparison to pyrophyllite. This result suggests that dehydroxylation is not a homogeneous process. A model for dehydroxylation of muscovite was developed from Pauling bond-strength summation calculations. The strength of the Al–OH bond is greatly affected by the coordination number of neighboring polyhedra. When neighboring polyhedra are in octahedral coordination, the hydroxyl group is lost at lower temperatures than when neighboring polyhedra are in fivefold coordination (after partial dehydroxylation). This effect results from the distribution of oversaturated apical oxygens that affect also the proton position and the Al–OH bond strength. The model is applicable to pyrophyllite and similar dioctahedral 2:1 layer silicates and is supported by previously reported infrared, NMR, and TEM data.

INTRODUCTION

Unlike other rock-forming silicates, high-temperature structural studies of the hydrous layer-silicate minerals have not been undertaken, possibly because of the difficulties associated with partial hydroxyl loss at elevated temperatures. In order to avoid such complications, Takeda and Morosin (1975) studied synthetic fluorphlogopite-1M to 700°C, well below its decomposition temperature of about 1200°C. They found that the *c*-axis length increased at a rate nearly twice that of the other axes and that the Mg octahedra elongated more rapidly parallel to Z^* than other directions above approximately 400°C. In addition, they found that the tetrahedral sheet became more nearly hexagonal and that the M(2) site became larger than M(1) near 700°C.

These results have important implications in the formation of polytypes, in the mechanisms of thermal decomposition, and in cation-ordering effects. Takeda and Morosin (1975) suggested that polytype formation of high-temperature trioctahedral micas might not be related to the spatial relationship of tetrahedra around the interlayer cation as had been suggested earlier by Takeda et al. (1971). Takeda and Morosin argued that if the tetrahedral sheet approaches hexagonal symmetry at high temperatures, then the interlayer cation would have very similar environments regardless of polytype.

Takeda and Morosin (1975) stated that thermal decomposition resulted from the loss of contact of the anions around the interlayer cations, but Hazen (1977) concluded that misfit between the tetrahedral and octahedral sheets is an important consideration for the stability of the biotite series of micas. The basis of the argument is that if the tetrahedral sheet becomes hexagonal and fully extended laterally at high temperature, the tetrahedral sheet cannot remain congruent with the laterally expanding octahedral sheet at even higher temperatures. Toraya

0003–004X/87/0506–0537$02.00

(1981) discussed relative thermal stability of mica structures as a function of the variation of the size and shape of the octahedra. He did note, however, that a fully extended tetrahedral sheet may not be the only condition for establishing an upper temperature limit of decomposition. Because of the widespread implications of the fluorphlogopite refinement, the present study was undertaken to provide structural and thermal-analysis information on muscovite, a hydroxyl-rich, dioctahedral mica. On the basis of the data, a structural model for the dehydroxylation of muscovite is presented. Initially, only muscovite was considered in the model development, but it is apparent that the model may be expanded to include pyrophyllite and other dioctahedral 2:1 layer silicates. These models satisfy the structural, thermal, infrared, TEM (transmission-electon microscopy), and NMR (nuclear magnetic resonance) data of muscovite and pyrophyllite.

Previous work

Muscovite and pyrophyllite, which are believed to have similar dehydroxylation processes, have been studied by differential thermal analysis (DTA) by many workers (e.g., Grim et al., 1951; MacKenzie and Milne, 1953; Grim, 1968; and many others). Both phases behave similarly, with reaction peaks showing very broad widths indicating dehydroxylation over a range of 150–250 deg. With the development of very sensitive, commercially available thermal-analysis equipment, MacKenzie et al. (1985) found two distinct but overlapping peaks in the thermal analysis of pyrophyllite. They interpreted the first peak, centered at about 520°C, as due to *interlayer* water loss, whereas the second peak, centered at about 673°C, is caused by dehydroxylation. They suggested that water loss at about 520°C represents approximately 30% of the total hydroxyl water present. Such an interpretation seems unlikely for several reasons: (1) Lee and Guggenheim (1981) found no evidence of interlayer water in an X-ray crystal-structure refinement of pyrophyllite, even after a difference Fourier electron-density map was examined. (2) There are no interlayer sites for H_2O in pyrophyllite of the type occupied by K in muscovite, since adjacent 2:1 layers are offset within the (001) plane in pyrophyllite relative to muscovite. (3) For various cation-exchanged montmorillonites, in which interlayer water is known to exist, interlayer dehydration has been shown to occur at 1 atm at well below 200°C (Koster van Groos and Guggenheim, 1984, 1986, 1987). By comparison, pyrophyllite, which has neutral 2:1 layers, would be expected to lose its interlayer water at lower temperatures, if interlayer water is present. No recent thermal-analysis curves for muscovite are available in the published literature, and this paper presents such data for comparison to pyrophyllite.

Both the crystal structures of pyrophyllite and muscovite alter at high temperatures to a metastable dehydroxylate phase. The dehydroxylation reaction for these minerals may be given as $2(OH) \rightarrow H_2O(\uparrow) + O$, where the residual oxygen moves to the z-coordinate position of the Al cation. (For pyrophyllite dehydroxylate, see Wardle and Brindley, 1972, and for muscovite dehydroxylate, see Udagawa et al., 1974.) In the dehydroxylate phases, the Al cation is in fivefold coordination. Wardle and Brindley (1972) described this reaction as being homogeneous (as defined by Taylor, 1962) with adjacent pairs of $(OH)^-$ ions reacting as described above. In this case, "homogeneous" implies that dehydroxylation occurs uniformly throughout the crystal because all OH groups in the low-temperature form are thought to be identical. However, evidence for nonhomogeneous (i.e., not homogeneous) dehydroxylation was obtained from a Mössbauer study of Fe-containing muscovite (Heller-Kallai and Rozenson, 1980) in which it was concluded that dehydroxylation did not occur uniformly throughout their Fe-containing material.

Infrared data for muscovite (e.g., Gaines and Vedder, 1964; Aines and Rossman, 1985) show a small amount of peak broadening and a small wave-number shift from 3628 cm^{-1} to about 3600 cm^{-1} for O–H absorption during dehydroxylation, along with a decrease in intensity. Peak breadth and position and intensity recover to near original positions and intensity after the sample is placed under water pressure (Gaines and Vedder, 1964; Vedder and Wilkins, 1969) or exposed to laboratory conditions (Aines and Rossman, 1985) prior to re-examination.

Freund (1974) suggested from infrared data a proton-tunneling process for $Mg(OH)_2$ that has been extended to muscovite by Wirth (1985) on the basis of sheet distortions as observed by TEM. Such observations, however, may have many possible causes including partial hydroxyl loss, differential heating, and beam-induced damage. Also, a similar mechanism of dehydroxylation for muscovite and $Mg(OH)_2$ would be surprising because the structures are very different. The $Mg(OH)_2$ structure is not dioctahedral nor are the octahedral polyhedra linked to silicate sheets as they are in muscovite, and $Mg(OH)_2$ has a different hydroxyl topology than muscovite. In addition, because variations in the infrared patterns between the low-temperature muscovite form and the dehydroxylate are relatively small, Aines and Rossman (1985) suggested that water molecules form by simple diffusional hopping of H^+ to an adjacent OH^- site.

Although muscovite high-temperature forms have not been studied by NMR, MacKenzie et al. (1985) examined pyrophyllite magic-angle ^{27}Al NMR and ^{29}Si NMR spectra in addition to thermal-analysis data. Frost and Barron (1984) presented similar spectra, but with less detail, and unlike MacKenzie et al. (1985), they did not develop a model to explain their results. Therefore, because we seek to understand the process of dehydroxylation, the discussion emphasizes the data and results of MacKenzie et al. Spectra (MacKenzie et al., 1985) taken from quenched thermal experimental runs show that the Si-resonance peak at a chemical shift of about 100 ppm characteristic of the dehydroxylate phase occurs even at 565°C (at the

completion of the 520°C endotherm). These data appear to contradict their conclusion that the 520°C endotherm is related to interlayer-water loss. MacKenzie et al. felt, however, that this conclusion could be justified on the basis that the pyrophyllite dehydroxylate contribution to this spectrum appears relatively small. They considered also models for water loss at temperatures above 900°C for the remaining few percent of water. A prominent feature of the ^{27}Al NMR spectra is the marked decrease in peak areas with thermal treatment. They noted that this feature is common to other hydrous aluminosilicates, and they attributed it to the defect nature of the phases or distortions in the component anion polyhedra. For the ^{27}Al NMR spectrum taken at 565°C, they stated that the spectrum is unchanged from the unheated sample, although small intensity variations (at chemical shifts near 60 and 70 ppm) characteristic of the stronger peaks of the dehydroxylate are obvious in their figures. Peak overlap with the low-temperature form may partly mask other intensity variations. Attempts by MacKenzie et al. to correlate ^{27}Al NMR spectra to structural parameters such as Al–O bond lengths were not successful.

TABLE 1. Electron-microprobe data for muscovite from Keystone, South Dakota, and Panasqueira, Portugal

	Keystone			Panasqueira		
Oxide	Wt%	Cations per 11 oxygens		Wt%	Cations per 11 oxygens	
SiO_2	45.54	3.10	^{iv}4.00	46.16	3.09	^{iv}4.00
Al_2O_3	34.05	^{iv}0.90, ^{vi}1.83		36.08	^{iv}0.91, ^{vi}1.93	
FeO	2.74	0.16		0.25	0.01	
MgO	0.12	0.01	^{vi}2.01	00.10	0.01	^{vi}1.96
TiO_2	b.d.			b.d.		
MnO	0.16	0.01		0.12	0.01	
Na_2O	0.63	0.08		0.24	0.03	
CaO	0.16	0.01	^{xii}1.02	0.15	0.01	^{xii}1.04
K_2O	10.76	0.93		11.68	1.00	
F	0.91			0.58		
Total	95.11			95.36		

Note: An Applied Research Laboratories SEMQ microprobe was used to determine F by using a synthetic fluorphlogopite as a standard at the following operating conditions: 15-kV beam defocused at 10 μm to avoid sample damage and 30-s count collection at each point. E. Glover, analyst. A JEOL JSM-35CF and Tracor Northern 5500 Microtrace EDS was used at 15 kV with a beam current of about 300 pA, at 100 s per point, to determine the remaining chemistry. Standards included quartz, Si; synthetic corundum, Al; magnetite (USNM 114837), Fe; synthetic periclase, Mg; synthetic rutile, Ti; spessartine, Mn; albite, Na; wollastonite, Ca; microcline (USNM 143996), K. G. Harris, analyst. b.d. = below detection.

EXPERIMENTAL DETAILS

X-ray study

Data collection. Crystals from two sources were used in the study at high temperatures. Muscovite-2M_1 from the Diamond mine, Keystone, South Dakota, was used for the structural determination at 20°C and 300°C and for cell-dimension refinements to 1000°C. In addition, structural determinations at 20, 525, and 650°C and cell-dimension measurements to 650°C were made on muscovite-2M_1 from Panasqueira, Portugal. Elasticity measurements were reported recently by Vaughan and Guggenheim (1986) for the latter sample. The Keystone muscovite crystal used to obtain cell parameters to 1000°C was 0.25 × 0.25 × 0.03 mm in size, whereas the other used for one 20°C and the 300°C structural determinations was 0.25 × 0.28 × 0.03 mm. Both were cleavage fragments cut from the same flake. The Panasqueira sample had {010} and {110} growth faces and (001) cleavage and was 0.40 × 0.38 × 0.30 mm in size. Table 1 presents chemical information. The structural formula for the Keystone sample is $(K_{0.93}Na_{0.08}Ca_{0.01})(Al_{1.83}Fe_{0.16}Mg_{0.01})(Si_{3.10}Al_{0.90})O_{10}(OH)_{1.83}F_{0.17}$, and for the Panasqueira sample, the structural formula is $(K_{1.00}Na_{0.03}Ca_{0.01})(Al_{1.93}Fe_{0.01}Mg_{0.01}Mn_{0.01})(Si_{3.09}Al_{0.91})O_{10}(OH)_{1.88}F_{0.12}$.

Crystals were examined by the precession method to determine space group and crystal quality. Both samples were found to crystallize in *C*2/*c* symmetry. The Keystone crystal has a moderate amount of mosaic spread, whereas the Panasqueira crystal has a *slight* diffuseness parallel to **c*** for $k \neq 3n$ reflections, indicating that there is minor stacking disorder.

A Picker four-circle, single-crystal X-ray diffractometer with graphite-monochromatized Mo$K\alpha$ radiation was used with a single-crystal heater (Brown et al., 1973). The heater was calibrated in a manner similar to that reported by Brown et al. (1973) with substances of known melting points ($C_7H_6O_3$ at 158°C, $NaNO_3$ at 306°C, $BaNO_3$ at 592°C, NaI at 561°C, and KCl at 790°C). Experiments to determine temperature variability at different crystal settings on the four-circle diffractometer indicated stability to be ±2% at 800°C. Temperature variations within the room were ±3°C. Therefore, total associated temperature error is believed to be approximately ±8°C at 300°C, ±11°C at 525°C, and ±13°C at 650°C. Errors from thermocouple calibration or variations in applied voltage to the heater are considered negligible in comparison. Small systematic errors in each high-temperature data set are expected because temperatures vary within the stated extremes at diffractometer settings of $\chi = 90°$ vs. $\chi = 0°$ or 180°.

Crystals used in the high-temperature refinements were cemented to the ends of quartz-glass fibers with Zircoa Bond 6 cement and ground quartz-glass wool and then were inserted into a 0.5-mm-diameter quartz-glass capillary. For the Keystone muscovite experiments, each crystal was cemented to the fiber on the (001) cleavage plane, and no cement was allowed to touch the other sides of the crystal. The cement was cured at 150°C for 30 min prior to sealing the capillary tube in an evacuated state. The Panasqueira crystal, although mounted also on the (001) face, was treated differently. Cement was applied to two opposing edges of the crystal for greater adherence because cement failure prevented the completion of the heating experiments on the Keystone samples. In addition, curing time was extended to 2 h.

Unit-cell parameters (Table 2) of the Keystone crystal were determined by least-squares refinement of 27 medium-angle ($30° < 2\theta < 45°$), auto-centered (Lenhert, 1975) reflections. The cell parameters from the Panasqueira crystal were determined from 15 high-angle reflections with a Krisel control system. For the Panasqueira sample and for temperatures (20, 525, 650°C) at which a structure was completed, the 15 high-angle reflections were measured in eight equivalent positions, resulting in the use of 120 reflection observations. In order to avoid hysteresis effects, the crystal under observation was slowly heated to temperature and never allowed to overshoot. Usually each temperature setting was held for a minimum of 12 h prior to data collection for cell parameters or 24 h prior to structural data collection.

Data sets for the structural refinement of the Keystone muscovite were obtained with a stationary counter while the crystal was being rotated through 1.6° by a continuous ω scan mode at

TABLE 2. Unit-cell parameter data for muscovite to 1000°C

Temperature (°C)	a (Å)	b (Å)	c (Å)	β (°)	V (Å³)
	Muscovite, Panasqueira, Portugal				
20	5.1579(9)	8.9505(8)	20.071(5)	95.75(2)	921.9(3)
200	5.168(1)	8.9603(7)	20.112(7)	95.74(3)	926.7(4)
250	5.169(2)	8.9654(6)	20.141(6)	95.74(3)	928.6(4)
300	5.170(1)	8.970(1)	20.171(6)	95.71(3)	930.8(4)
350	5.173(1)	8.971(1)	20.174(8)	95.73(3)	931.6(4)
400	5.175(2)	8.9763(8)	20.177(9)	95.72(3)	932.6(5)
450	5.178(1)	8.9835(9)	20.193(6)	95.70(2)	934.7(3)
525	5.182(1)	8.993(1)	20.232(5)	95.75(2)	938.2(3)
650	5.189(1)	9.004(1)	20.256(6)	95.74(2)	941.8(4)
	Muscovite, Diamond mine, Keystone, South Dakota				
20	5.200(4)	9.021(7)	20.07(2)	95.71(7)	937(1)
100	5.202(2)	9.030(2)	20.079(7)	95.67(2)	938.6(5)
200	5.210(2)	9.043(3)	20.125(9)	95.71(2)	943.5(6)
300	5.215(2)	9.053(4)	20.15(1)	95.72(3)	946.7(7)
400	5.221(2)	9.067(4)	20.18(1)	95.73(3)	950.5(7)
430	5.222(3)	9.067(4)	20.18(1)	95.64(3)	951.0(8)
500	5.225(3)	9.073(5)	20.20(1)	95.79(4)	952.7(9)
600	5.229(4)	9.081(6)	20.24(2)	95.92(5)	956(1)
650	5.233(2)	9.086(3)	20.25(1)	95.62(3)	957.9(7)
700	5.235(3)	9.091(4)	20.26(1)	95.73(3)	959.5(8)
750	5.237(2)	9.095(4)	20.26(1)	95.73(3)	959.9(7)
800	5.240(2)	9.102(3)	20.28(1)	95.73(3)	962.5(7)
900	5.241(5)	9.122(8)	20.35(2)	96.14(7)	967(2)
1000	5.25(1)	9.21(2)	20.44(7)	96.2(2)	981(4)

1°/min and with 20 s per background measurement (Lenhert, 1975). Reflections for half of the reciprocal sphere were collected with the approximate range of h from -7 to 7, k from -12 to 12 and l from 0 to 30. Crystal and electronic stability was monitored by comparing the intensities of three reflections, measured every 3 h during data collection. The standard deviation of an intensity measurement was computed from $\sigma(I) = [CT + 0.25(t_c/t_b)^2(B_1 + B_2) + (pI)^2]^{1/2}$ where CT is the total integrated count in time t_c, B_1 and B_2 are the background counts in time t_b, and p (the estimate of the standard error) is equal to 0.03. Reflections were considered observed if the intensities were greater than 3σ. The data were corrected for Lorentz-polarization and absorption effects; the latter was made empirically (North et al., 1968) with complete ψ scans (0°–360° at 10° increments in ϕ) of reflections at about 5° intervals in 2θ. The ψ scans were measured at room temperature only but were also applied to the high-temperature data set. Of the 1855 reflections collected at room temperature, there were 963 unique nonzero intensities after symmetry averaging into two octants. The high-temperature data set resulted in 1282 unique nonzero intensities from a total collected set of 2411.

Thermocouple failure prevented an accurate temperature determination for the Keystone muscovite high-temperature experiment. The measured cell parameters were $a = 5.222(2)$, $b = 9.063(4)$, $c = 20.09(3)$ Å, $\beta = 95.75(3)°$ with a volume of 946.13 Å³. These results suggest a temperature of approximately 300°C when compared to the volume of 946.71 Å³ determined at that temperature.

Data sets for the structural refinement of the Panasqueira sample follow similar collection procedures as above, except that a $2\theta{:}\theta$ fixed-scan mode with a window of 1° 2θ and with 10 s per background count was used. Because of the larger crystal size of the Panasqueira sample, many more reflections were collected: 3563 for the room-temperature refinement, 3148 for the 525°C refinement, and 3159 for the 650°C refinement, with resulting data sets after symmetry averaging of 1351, 1358, and 1336 reflections, respectively.

Refinement. Initial atomic parameters for the room-temperature refinement were obtained from Rothbauer (1971). Atoms were considered half-ionized, and scattering factors were calculated from Cromer and Mann (1968). Because of the slight diffuseness of some of the reflections in the Panasqueira sample, intensity calculations for $k = 3n$ and $k \neq 3n$ reflections for that sample were made with separate scale factors. The scale factor(s) and nonfixed atomic positions in space group $C2/c$ were varied first, followed by isotropic temperature factors and then anisotropic temperature factors. Reflections were given unit weights, and a modified least-squares program ORFLS (Busing et al., 1962) was used. Twelve reflections were removed from the data set of each of the Panasqueira refinements due to considerable primary extinction. A secondary extinction correction was made. A difference electron-density map was made at the end of each series of refinements. The refinements of the Panasqueira crystal showed that approximately one-half of an electron is present on the average in the normally vacant M(1) octahedral site, but this result was not included in the refinement process. No attempt was made to locate the H position. All other atom locations on the difference electron-density map appeared flat, and there was no evidence suggesting that the high-temperature studies involved dehydroxylation. The results of each refinement are given in Table 3. Final atomic and thermal parameters are listed in Table 4. Values of F_o and F_c are listed[1] in Table 5.

Thermal analysis

Thermogravimetric analyses (TGA, DTG) were done on a Dupont 1090 analyzer in N_2 atmosphere at the Department of Earth Sciences of the University of Utrecht, the Netherlands (Fig. 1A).

[1] To obtain copies of Tables 5 and 9, order Document AM-87-338 from the Business Office, Mineralogical Society of America, 1625 I Street, N.W., Suite 414, Washington, D.C. 20006, U.S.A. Please remit $5.00 in advance for the microfiche.

TABLE 3. Results of the structural refinements at various temperatures

	Panasqueira, Portugal			Keystone, South Dakota	
	20°C	525°C	650°C	20°C	300°C
R_1*	0.052	0.069	0.071	0.040	0.053
wR†	0.057	0.071	0.073	0.046	0.068
Goodness-of-fit‡	1.38	1.83	1.84	1.66	2.67
Variable parameters	89	89	89	87	87
Data set	1339	1346	1324	963	1282

* $R_1 = (\Sigma||F_o| - |F_c||)/\Sigma|F_o|$.
† $wR = \{[w(|F_o| - |F_c|)^2]/\Sigma w|F_o|^2\}^{1/2}$ where $w = 1$.
‡ Goodness-of-fit $= [\Sigma w||F_o| - |F_c||^2/\Sigma(n - m)]^{1/2}$, where n = number of independent data and m = number of parameters.

TABLE 4. Positional coordinates and thermal parameters

Atom	x	y	z	B_{eq}†	β_{11}	β_{22}	β_{33}	β_{12}	β_{13}	β_{23}
Muscovite, Keystone, South Dakota										
at 20°C										
K	0.0	0.0982(3)	0.25	1.68	0.0147(8)	0.0058(3)	0.00099(5)	0.0	0.0003(2)	0.0
Al	0.2511(4)	0.0836(2)	0.0001(1)	0.64	0.0039(5)	0.0022(2)	0.00047(4)	−0.0010(3)	0.0001(1)	0.00008(8)
T(1)	0.4648(3)	0.9294(2)	0.13565(9)	0.62	0.0043(6)	0.0018(2)	0.00051(4)	−0.0004(3)	0.0001(1)	0.00009(8)
T(2)	0.4517(3)	0.2584(2)	0.13545(9)	0.63	0.0043(6)	0.0021(2)	0.00047(4)	−0.0003(3)	0.0001(1)	−0.00009(9)
O(1)	0.4170(9)	0.0926(5)	0.1683(2)	1.20	0.013(2)	0.0029(5)	0.0008(1)	−0.0007(9)	0.0005(3)	−0.0001(2)
O(2)	0.251(1)	0.8112(5)	0.1582(3)	1.42	0.012(2)	0.0042(6)	0.0010(1)	−0.0006(9)	−0.0000(4)	0.0006(2)
O(3)	0.251(1)	0.3705(5)	0.1690(2)	1.24	0.010(2)	0.0042(6)	0.0008(1)	0.0026(8)	0.0002(3)	−0.0001(2)
O(4)	0.4579(8)	0.9438(5)	0.0536(2)	0.84	0.003(2)	0.0028(5)	0.0008(1)	−0.0003(7)	−0.0001(3)	0.0001(2)
O(5)	0.3858(8)	0.2528(6)	0.0537(2)	1.06	0.007(1)	0.0035(5)	0.0008(1)	0.0004(9)	0.0003(3)	0.0002(2)
OH	0.4565(9)	0.5636(5)	0.0503(2)	0.95	0.008(2)	0.0037(5)	0.0005(1)	−0.0011(8)	0.0005(3)	−0.0002(2)
at 300°C										
K	0.0	0.0982(5)	0.25	2.76	0.024(2)	0.0090(6)	0.0017(1)	0.0	0.0009(3)	0.0
Al	0.2511(6)	0.0835(3)	0.0000(1)	0.95	0.0072(8)	0.0029(3)	0.0007(1)	−0.0008(5)	0.0005(2)	0.0002(1)
T(1)	0.4645(5)	0.9297(3)	0.1351(1)	0.86	0.0058(8)	0.0025(3)	0.0007(1)	−0.0000(5)	0.0005(2)	0.0000(1)
T(2)	0.4514(5)	0.2584(3)	0.1354(1)	0.86	0.0059(8)	0.0025(3)	0.0007(1)	−0.0000(5)	0.0004(2)	0.0000(1)
O(1)	0.423(1)	0.0939(9)	0.1684(3)	1.50	0.016(3)	0.0045(8)	0.0008(2)	−0.001(1)	0.0001(5)	0.0003(3)
O(2)	0.247(1)	0.8127(9)	0.1570(4)	1.92	0.013(3)	0.0064(9)	0.0014(2)	−0.003(1)	−0.0002(5)	0.0007(4)
O(3)	0.248(1)	0.3675(8)	0.1682(4)	1.82	0.015(3)	0.0049(9)	0.0014(2)	0.003(1)	0.0007(6)	0.0000(4)
O(4)	0.461(1)	0.9439(8)	0.0540(4)	1.21	0.009(2)	0.0042(8)	0.0008(2)	0.000(1)	0.0011(5)	0.0004(3)
O(5)	0.384(1)	0.2517(8)	0.0530(3)	1.17	0.010(2)	0.0045(8)	0.0006(2)	0.001(1)	0.0003(4)	0.0005(4)
OH	0.455(1)	0.5624(8)	0.0505(4)	1.41	0.010(3)	0.0042(9)	0.0011(2)	0.000(1)	0.0010(6)	−0.0003(3)
Muscovite, Panasqueira, Portugal										
at 20°C										
K	0.0	0.0989(2)	0.25	1.79	0.0166(4)	0.0062(2)	0.00103(3)	0.0	0.00019(9)	0.0
Al	0.2509(2)	0.0836(1)	0.00002(5)	0.68	0.0048(3)	0.0021(1)	0.00054(2)	−0.0004(1)	−0.00007(6)	0.00004(4)
T(1)	0.4649(2)	0.9297(1)	0.13481(5)	0.72	0.0059(3)	0.0022(1)	0.00053(2)	−0.0000(1)	−0.00004(6)	0.00003(4)
T(2)	0.4516(2)	0.2584(1)	0.13495(5)	0.77	0.0062(3)	0.0026(1)	0.00051(2)	−0.0002(1)	−0.00015(6)	−0.00000(4)
O(1)	0.4133(6)	0.0924(3)	0.1672(1)	1.37	0.016(1)	0.0036(3)	0.00080(6)	0.0003(4)	0.0005(2)	0.0001(1)
O(2)	0.2521(5)	0.8099(3)	0.1569(1)	1.46	0.0108(9)	0.0058(3)	0.00087(6)	−0.0021(5)	−0.0005(2)	0.0003(1)
O(3)	0.2517(5)	0.3712(3)	0.1678(1)	1.28	0.0103(9)	0.0049(3)	0.00074(6)	0.0020(4)	−0.0003(2)	−0.0003(1)
O(4)	0.4618(5)	0.9435(3)	0.0532(1)	0.82	0.0057(7)	0.0028(3)	0.00061(5)	0.0008(4)	−0.0002(2)	0.0002(1)
O(5)	0.3843(5)	0.2520(5)	0.0532(1)	0.84	0.0081(8)	0.0026(3)	0.00052(5)	0.0000(4)	−0.0000(2)	0.0002(1)
OH	0.4575(5)	0.5618(3)	0.0499(1)	0.92	0.0073(8)	0.0031(3)	0.00063(6)	−0.0004(4)	0.0001(2)	−0.0003(1)
at 525°C										
K	0.0	0.0983(3)	0.25	3.76	0.0348(9)	0.0127(3)	0.00214(5)	0.0	0.0009(2)	0.0
Al	0.2512(2)	0.0833(1)	0.00013(7)	1.14	0.0089(4)	0.0034(1)	0.00085(3)	−0.0005(2)	0.00014(8)	0.00011(5)
T(1)	0.4644(2)	0.9300(1)	0.13402(6)	1.12	0.0094(4)	0.0033(1)	0.00079(3)	−0.0003(2)	0.00027(7)	0.00014(4)
T(2)	0.4510(2)	0.2589(1)	0.13416(6)	1.20	0.0103(4)	0.0037(1)	0.00080(3)	−0.0003(2)	−0.00000(8)	0.00006(5)
O(1)	0.4226(8)	0.0933(4)	0.1666(2)	2.17	0.028(1)	0.0049(4)	0.00121(8)	0.0001(6)	0.0014(3)	−0.0001(1)
O(2)	0.2451(7)	0.8156(5)	0.1563(2)	2.49	0.018(1)	0.0097(5)	0.00150(9)	−0.0043(7)	−0.0004(3)	0.0008(2)
O(3)	0.2456(7)	0.3664(4)	0.1669(2)	2.14	0.017(1)	0.0081(5)	0.00123(8)	0.0042(6)	−0.0006(2)	−0.0005(2)
O(4)	0.4617(6)	0.9439(4)	0.0531(2)	1.48	0.010(1)	0.0056(4)	0.00097(7)	0.0012(5)	0.0003(2)	0.0004(1)
O(5)	0.3830(6)	0.2522(3)	0.0530(2)	1.40	0.015(1)	0.0039(3)	0.00083(7)	0.0009(5)	−0.0002(2)	0.0003(1)
OH	0.4568(6)	0.5622(4)	0.0497(2)	1.59	0.011(1)	0.0055(4)	0.00112(7)	−0.0017(5)	0.0007(2)	−0.0004(1)
at 650°C										
K	0.0	0.0985(3)	0.25	4.35	0.041(1)	0.0146(4)	0.00243(6)	0.0	0.0009(2)	0.0
Al	0.2511(3)	0.0835(1)	0.00002(7)	1.28	0.0102(4)	0.0038(2)	0.00094(3)	−0.0003(2)	0.00017(8)	0.00015(5)
T(1)	0.4637(2)	0.9302(1)	0.13393(6)	1.24	0.0109(4)	0.0036(1)	0.00086(3)	−0.0001(2)	0.00037(8)	0.00015(5)
T(2)	0.4515(2)	0.2591(1)	0.13383(6)	1.35	0.0114(4)	0.0042(1)	0.00091(3)	−0.0001(2)	0.00005(8)	0.00005(5)
O(1)	0.4253(8)	0.0931(4)	0.1662(2)	2.44	0.032(2)	0.0054(4)	0.00133(9)	−0.0002(7)	0.0013(3)	0.0002(2)
O(2)	0.2429(8)	0.8178(5)	0.1560(2)	2.87	0.022(1)	0.0113(6)	0.0016(1)	−0.0052(8)	−0.0006(3)	0.0009(2)
O(3)	0.2451(7)	0.3652(5)	0.1669(2)	2.36	0.018(1)	0.0097(5)	0.00124(8)	0.0042(7)	−0.0005(3)	−0.0007(2)
O(4)	0.4621(6)	0.9438(4)	0.0530(2)	1.61	0.012(1)	0.0061(4)	0.00096(7)	0.0010(5)	0.0005(2)	0.0003(1)
O(5)	0.3822(7)	0.2520(4)	0.0530(2)	1.56	0.017(1)	0.0043(3)	0.00090(7)	0.0010(5)	−0.0001(2)	0.0002(1)
OH	0.4564(6)	0.5624(4)	0.0496(2)	1.79	0.014(1)	0.0059(4)	0.00120(8)	−0.0022(5)	0.0013(2)	−0.0003(1)

† B_{eq} is calculated from $\frac{4}{3}[\beta_{11}/(a^*)^2 + \beta_{22}/(b^*)^2 + \beta_{33}/(c^*)^2]$. The anisotropic temperature factor form is $\exp(-\Sigma_i\Sigma_j\Sigma_{ij}h_ih_j)$.

Figure 1B provides similar data for pyrophyllite from MacKenzie et al. (1985).

The thermal-analysis curves for muscovite show a small weight loss (~1%) at low temperatures, which may be attributed to absorbed surface-water effects. Between 475 and 950°C, a large and asymmetric peak occurs, which is interpreted as a result of dehydroxylation. Because of the similarities in the crystal structure of muscovite and pyrophyllite and their respective dehydroxylates, comparison of the muscovite and pyrophyllite data is justified. Note that the asymmetric nature of the muscovite peak (between 475 and 950°C) closely resembles the pyrophyllite data (see the region between 475 and 800°C) except that in pyrophyllite two peaks are resolved (centered at 520°C and 673°C). Thus, similar to pyrophyllite, muscovite dehydroxylation also occurs as two major events (centered approximately at 550 and 750°C) although the events are not as well defined. Dehydroxyl-

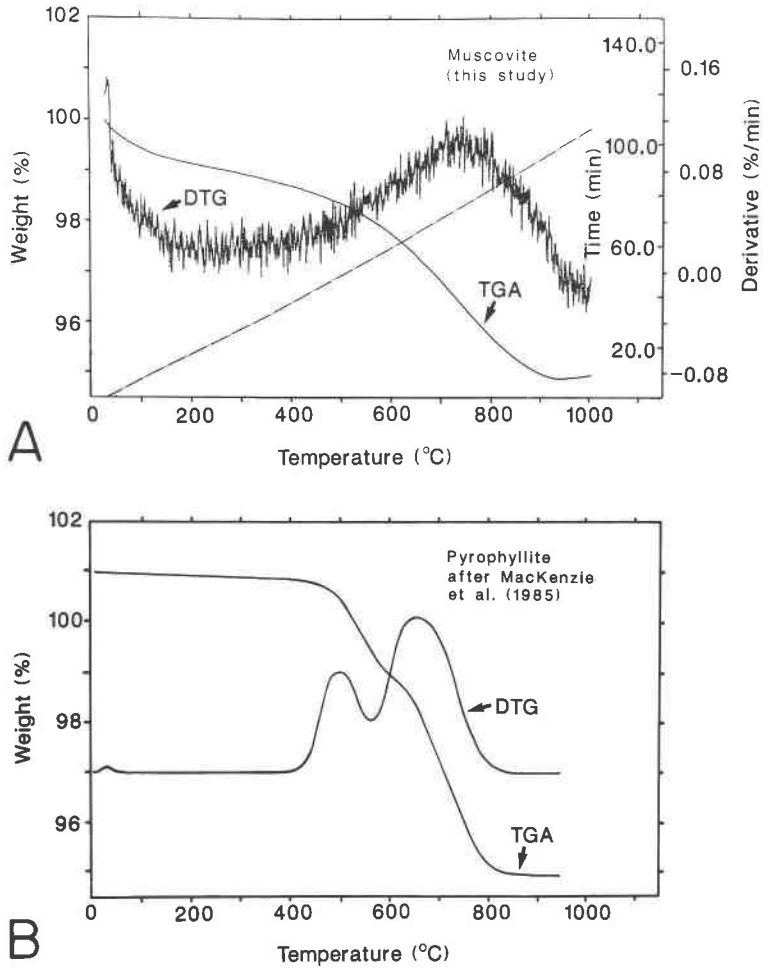

Fig. 1. TGA and DTG diagrams for muscovite (A) from Keystone, South Dakota, and pyrophyllite (B). The latter data are modified from MacKenzie et al. (1985).

ation in muscovite and pyrophyllite starts at about the same temperature (approximately 475°C), but the rate at which H_2O is lost is more rapid in pyrophyllite for each of the two major events.

Discussion

Unit-cell parameters

The chemical composition of the Panasqueira muscovite is very close to the composition of the end member. It is apparent that small substitutions of Fe^{2+} or Na have a pronounced effect on the a and b axial lengths (cf. Keystone muscovite). The Panasqueira muscovite has slightly smaller cell dimensions at room temperature than the synthetic muscovite-$2M_1$ ($a = 5.189, b = 8.995, c = 20.097$ Å, $\beta = 95.18°$) as reported by Yoder and Eugster (1955).

Figure 2 illustrates the effect of temperature on the unit-cell lengths and unit-cell volume. These data are consistent with those by Symmes (1986), who studied unit-cell expansion to 800°C. At temperatures above approximately 850°C, there is a marked change in slope and a large increase in the estimated standard deriations (esd's). This result is interpreted as due to a phase change to the (metastable) dehydroxylate form of muscovite (see Udagawa et al., 1974). Because of kinetic effects, the crystal decomposes at lower temperatures if the heating time is increased. Therefore, in order to avoid complications of collecting data and refining the structure of a crystal with a dehydroxylate phase, 650°C was not exceeded for the highest-temperature refinement. Note that Figure 2 (and other figures as well) assumes a linear extrapolation to 850°C. It is emphasized that a linear extrapolation is an assumption only and that the 850°C temperature limit is based on nonequilibrium conditions.

The mean thermal expansion coefficient (MTEC) of the c axis is substantially larger (by 1.5 times) than the axes within the basal plane (Table 6). This rapid increase in the c cell dimension dominates the observed volume expansion. The Panasqueira muscovite c-axis linear expansion appears to be greater than that of the Keystone sample, but Figure 2C illustrates error bars of only one esd.

The β angle and d_{001} distances are not illustrated in figure

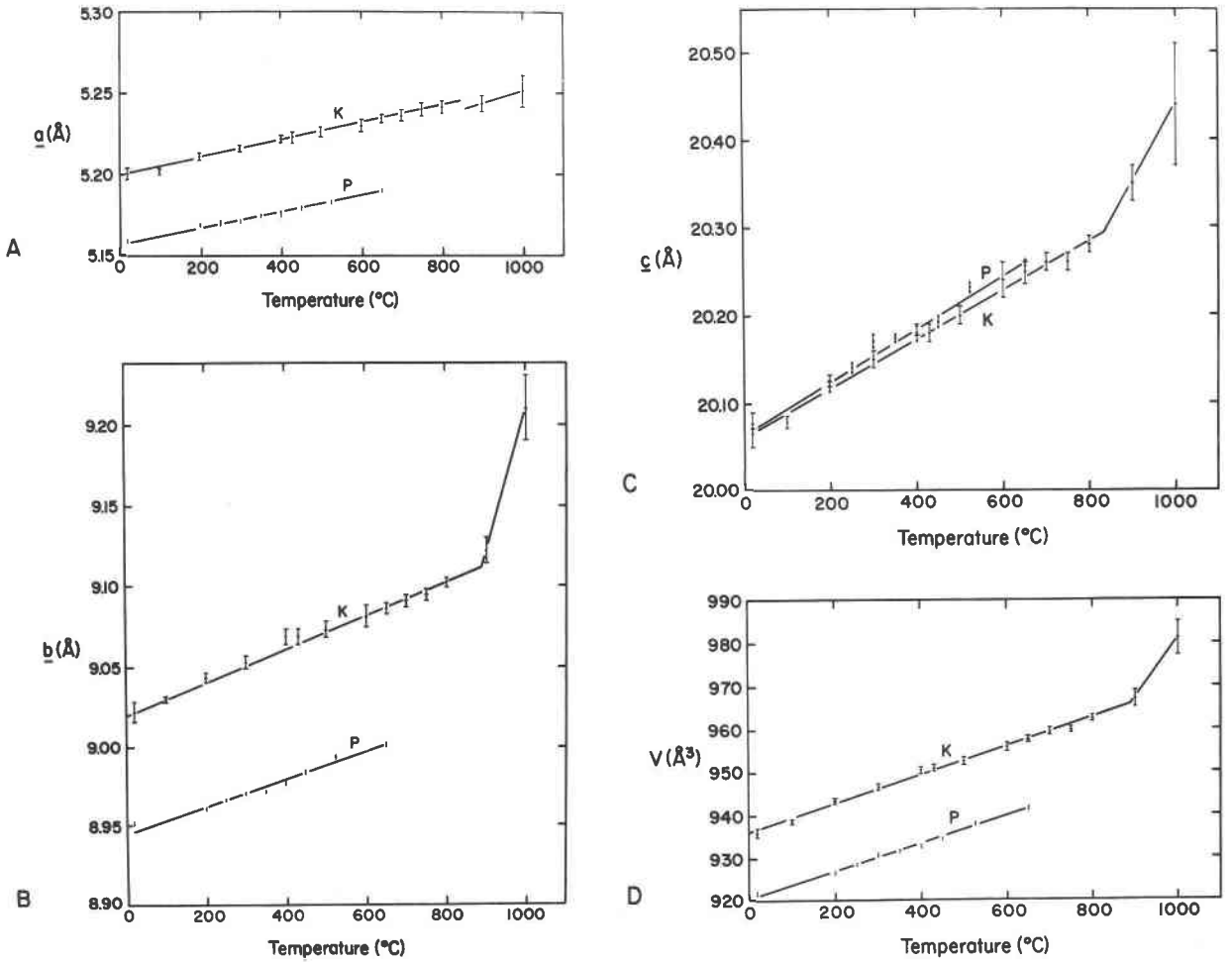

Fig. 2. Unit-cell and volume changes vs. temperature. One estimated standard deviation (esd) is shown, and symbols are K for muscovite from Keystone, South Dakota, and P for muscovite from Panasqueira, Portugal.

form. A plot of β vs. temperature indicated that β remains constant. The esd's associated with β for the Keystone muscovite are quite large, but they are much lower for the Panasqueira sample where the trend is more apparent. The plot of d_{001} vs. temperature is similar to c vs. temperature (Fig. 2); compare the MTEC values of c and d_{001}. This result is expected when the β angle does not change as a function of temperature, because d_{001} is equal to c sin β.

These results are in contrast to those found for fluorphlogopite (Takeda and Morosin, 1975). They found that the rate of expansivity for a and b decreased above 400°C, whereas the β-angle value decreased, and the c-axis expansivity remained nearly constant. They attributed these differences to the mode of octahedral distortion, where individual Mg octahedra elongate perpendicular to the layer above 400°C but do not change shape at lower temperatures. Because of the higher strength of Al–O bonds, such distortions may not be possible in Al-rich micas and are not observed in muscovite (see below).

Structural parameters

Bond lengths and angles (calculated from ORFEE, Busing et al., 1964) are presented in Table 7, and important polyhedral distances are plotted with respect to temperature in Figures 3 and 4. Additional structural parameters derived from the atomic coordinates are provided in Table 8. Polyhedral-site volumes, bond-angle variances, and quadratic elongations were calculated from the computer program VOLCAL of Finger and Ohashi as given in Hazen and Finger (1982).

The room-temperature refinements are in close agreement with other muscovite refinements (e.g., Rothbauer, 1971). The positional parameters (Table 4) of the high-temperature refinements (e.g., 650°C), which differ by more than 4 σ from the room-temperature refinement, are the z parameters of T(1) and T(2), the x parameters of O(1) and O(3), and the y parameters of O(2) and O(3). These oxygen anions represent the basal oxygen plane and are involved in the coordinating polyhedron of the interlayer cation. It is misleading, however, to consider just the atomic

TABLE 6. Mean thermal-expansion coefficients ($\times 10^{-5}$/deg)

	Key-stone α_{20-300}	Pana-squeira α_{20-650}		Key-stone α_{20-300}	Pana-squeira α_{20-650}
		Silicon tetrahedra			
T(1)–O(1)	3.047	0.000	T(2)–O(1)	−1.730	0.207
–O(2)	2.183	−0.104	–O(2)	−3.245	−1.074
–O(3)	0.431	0.482	–O(3)	−1.954	−0.139
–O(4)	−3.251	−0.001	–O(4)	3.698	0.139
Mean	0.651	0.139	Mean	−0.867	−0.277
Volume	3.133	0.000	Volume	−1.560	−1.258
	Al octahedron			Interlayer site (inner)	
Al–O(4)	0.000	0.942	K–O(1)	4.141	4.682
–O(5)	0.557	0.772	–O(2)	4.962	5.395
–OH	−0.554	0.951	–O(3)	5.263	4.542
–O(4)′	3.355	0.740	Mean	4.874	4.854
–O(5)′	−2.007	0.645	Volume	10.464	15.386
–OH′	2.783	1.159			
Mean	0.554	0.858			
Volume	1.513	2.477			
	Cell parameters				
	α_{20-800}	α_{20-650}			
a	0.994	0.928			
b	1.110	0.979			
c	1.379	1.502			
β	0.068	−0.019			
Volume	3.537	3.468			
d_{001}	1.367	1.505			

Note: Mean thermal-expansion coefficients, α, are calculated from $\alpha_x = (1/X_{20})/[(X_T - X_{20})/(T - 20)]$, where X_{20} and X_T are the values of the parameter at room temperature (20°C) and at a higher temperature, X_T. Whenever possible, α_x is calculated using the slope of the linear regression analysis for the term $[(X_T - X_{20})/(T - 20)]$.

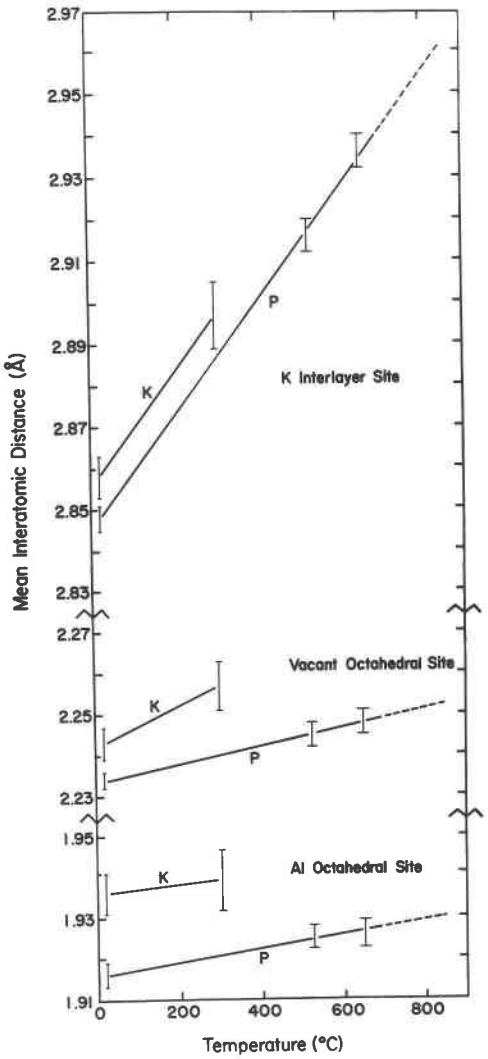

Fig. 3. Mean interatomic distances for cation polyhedra in muscovite vs. temperature. Symbols and esd as before.

coordinates to express thermally induced variations in the structure. It is necessary also to consider the effect of cell-parameter expansivity. For example, it is not readily apparent from examining basal-oxygen *z* fractional coordinates that the interlayer separation has increased significantly, as may be seen in Table 8.

Figure 3 shows that the interlayer-cation mean interatomic distance increases much more rapidly than the octahedral cation sites. At the same time, the interlayer separation increases, and the interlayer site changes shape (Table 8). The room-temperature structure shows that the octahedral interlayer K site (inner oxygens) is elongated parallel to Z^* and, consequently, the ψ value is less than the ideal value of 54°44′. With increasing temperature, ψ values increase, and the site becomes more ideal in shape (less elongate). In fluorphlogopite, this site is compressed ($\psi = 56.2°$) parallel to Z^* in the room-temperature structure with ψ values increasing with elevations in temperature (to $\psi = 56.5°$ at 700°C). Both sets of results suggest that the basal triads of the octahedron are increasing in size at a fast enough rate to offset any tendency for the interlayer site to become more elongate in shape parallel to Z^*, as might be expected as interlayer separation increases in an otherwise static structure.

Variations in individual interlayer bond lengths are given in Figure 4. The differences in the magnitudes of the individual distances remain similar as temperature increases. For example, the K–O(2) distance is the largest bond at room temperature and remains so at higher temperatures. The large size of K–O(2) and the higher rate of increase in length relative to the other K–O bonds indicate that this bond is weaker than either K–O(1) or K–O(3). In muscovite and other dioctahedral micas, the H^+ vector is influenced by the interlayer cation and the cation charges associated with the two filled M(2) octahedral sites. This arrangement tends to repulse the proton toward the portion of the structure with minimal local positive-charge concentration, namely the vacant M(1) octahedral site. For muscovite, Rothbauer (1971) found by neutron diffraction that the O–H vector is inclined from the (001) by about 12°. This vector points generally in the direction of the O(2) basal anion. In fact, the projection of the structure down Z^* shows that the oxygen associated with the proton, the proton, and O(2) form a straight line; see Figure 2 of Rothbauer (1971). The proximity of the proton

TABLE 7. Bond lengths and angles at various temperatures

	Bond lengths (Å)							Bond angles (°)				
	Keystone, South Dakota		Panasqueira, Portugal					Keystone, South Dakota		Panasqueira, Portugal		
	20°C	300°C	20°C	525°C	650°C			20°C	300°C	20°C	525°C	650°C
Al–O(4)	1.957(4)	1.957(7)	1.926(3)	1.938(3)	1.936(3)							
–O(5)	1.924(5)	1.927(8)	1.909(3)	1.917(3)	1.918(4)							
–OH	1.933(5)	1.930(8)	1.906(3)	1.916(3)	1.917(4)							
–O(4)′	1.916(5)	1.934(8)	1.913(3)	1.918(3)	1.923(4)							
–O(5)′	1.958(5)	1.947(8)	1.934(3)	1.942(3)	1.941(4)							
–OH′	1.925(5)	1.940(7)	1.906(3)	1.917(3)	1.920(3)							
Mean	1.936	1.939	1.916	1.925	1.926							
O(4)–O(4)′	2.455(6)	2.47(1)	2.430(4)	2.442(5)	2.441(5)	O(4)–Al–	O(4)′	78.6(2)	78.7(3)	78.5(1)	78.6(1)	78.5(1)
O(5)–O(5)′	2.457(6)	2.429(8)	2.428(3)	2.429(4)	2.429(5)	O(5)	O(5)′	78.5(2)	77.7(3)	78.4(1)	78.0(1)	78.0(1)
OH–OH′	2.404(6)	2.41(1)	2.366(4)	2.382(5)	2.383(5)	OH	OH′	77.1(2)	77.0(3)	76.7(1)	76.9(1)	76.8(2)
Mean (shared)	2.439	2.44	2.408	2.418	2.418			78.1	77.8	77.9	77.8	77.8
(edge with vacant site)												
O(4)–O(5)′	2.964(6)	2.96(1)	2.931(4)	2.951(4)	2.952(5)	O(4)–Al–	O(5)′	98.4(2)	98.7(3)	98.8(1)	99.1(1)	99.2(1)
O(4)′–OH	2.846(6)	2.87(1)	2.839(3)	2.851(4)	2.852(4)	O(4)′	OH	95.4(2)	95.9(3)	96.0(1)	96.1(2)	95.9(2)
O(5)–OH′	2.849(6)	2.87(1)	2.840(4)	2.852(4)	2.856(4)	O(5)	OH′	95.5(2)	95.7(3)	96.2(1)	96.1(1)	96.2(2)
(triad edges)												
O(4)′–O(5)′	2.815(6)	2.82(1)	2.790(4)	2.803(5)	2.805(5)	O(4)′–Al–	O(5)′	93.2(2)	93.1(3)	93.0(1)	93.1(1)	93.1(2)
–OH′	2.818(6)	2.844(9)	2.803(3)	2.819(4)	2.828(4)		OH′	94.4(2)	94.5(3)	94.4(1)	94.6(1)	94.7(2)
O(5)′–OH′	2.807(6)	2.816(9)	2.779(3)	2.788(4)	2.788(4)	O(5)′	OH′	92.6(2)	92.9(3)	92.7(1)	92.5(1)	92.4(2)
(triad edges)												
O(4)–O(5)	2.815(7)	2.815(9)	2.773(3)	2.782(4)	2.781(4)	O(4)–Al–	O(5)	93.0(2)	92.9(3)	92.6(1)	92.4(1)	92.4(2)
–OH	2.816(6)	2.804(9)	2.774(3)	2.784(4)	2.785(4)		OH	92.8(2)	92.4(3)	92.7(1)	92.5(1)	92.6(2)
O(5)–OH	2.831(7)	2.84(1)	2.800(4)	2.815(5)	2.823(5)	O(5)	OH	94.5(2)	95.0(3)	94.4(1)	94.5(1)	94.8(2)
Mean (unshared)	2.840	2.85	2.814	2.827	2.830			94.4	94.6	94.5	94.5	94.6
					Tetrahedron T(1)							
T(1)–O(1)	1.641(5)	1.655(8)	1.628(3)	1.632(4)	1.626(4)							
–O(2)	1.636(5)	1.646(8)	1.627(3)	1.630(4)	1.624(4)							
–O(3)	1.659(5)	1.661(8)	1.644(3)	1.644(4)	1.651(4)							
–O(4)′	1.648(5)	1.633(8)	1.642(3)	1.640(3)	1.643(3)							
Mean	1.646	1.649	1.635	1.637	1.636							
O(1)–O(2)	2.683(6)	2.71(1)	2.664(4)	2.662(5)	2.654(6)	O(1)–T(1)–	O(2)	110.0(3)	110.4(4)	109.8(2)	109.4(2)	109.5(2)
–O(3)	2.653(6)	2.66(1)	2.639(4)	2.639(5)	2.638(5)		O(3)	107.0(2)	107.0(4)	107.5(2)	107.3(2)	107.3(2)
–O(4)′	2.691(6)	2.69(1)	2.682(4)	2.685(5)	2.680(5)		O(4)′	109.8(2)	110.0(4)	110.3(1)	110.3(2)	110.2(2)
O(2)–O(3)	2.641(7)	2.65(1)	2.623(4)	2.621(5)	2.628(5)	O(2)	O(3)	106.6(3)	106.7(4)	106.6(2)	106.4(2)	106.8(2)
–O(4)′	2.727(7)	2.72(1)	2.717(4)	2.724(5)	2.722(5)		O(4)′	112.3(3)	112.2(4)	112.4(1)	112.8(2)	112.8(2)
O(3)–O(4)′	2.725(6)	2.70(1)	2.694(4)	2.697(5)	2.702(5)	O(3)	O(4)′	111.0(2)	110.3(4)	110.2(1)	110.4(2)	110.2(2)
Mean	2.687	2.69	2.670	2.671	2.671			109.5	109.4	109.5	109.4	109.5
					Tetrahedron T(2)							
T(2)–O(1)	1.652(5)	1.644(8)	1.640(3)	1.640(4)	1.643(4)							
–O(2)	1.651(5)	1.636(8)	1.634(3)	1.627(4)	1.622(4)							
–O(3)	1.645(5)	1.636(8)	1.629(3)	1.627(4)	1.628(4)							
–O(5)′	1.642(5)	1.659(6)	1.643(3)	1.647(3)	1.643(3)							
Mean	1.648	1.644	1.637	1.635	1.634							
O(1)–O(2)	2.652(6)	2.63(1)	2.638(4)	2.627(5)	2.630(6)	O(1)–T(2)–	O(2)	106.8(2)	106.7(4)	107.3(2)	107.1(2)	107.3(2)
–O(3)	2.653(6)	2.64(1)	2.631(4)	2.622(5)	2.623(6)		O(3)	107.2(2)	107.3(4)	107.2(1)	106.7(2)	106.6(2)
–O(5)′	2.706(6)	2.714(9)	2.688(4)	2.697(5)	2.693(5)		O(5)′	110.5(3)	110.5(4)	109.9(1)	110.3(2)	110.1(2)
O(2)–O(3)	2.687(7)	2.68(1)	2.669(4)	2.658(5)	2.649(5)	O(2)	O(3)	109.2(3)	110.0(4)	109.7(2)	109.5(2)	109.2(2)
–O(5)′	2.737(7)	2.73(1)	2.720(4)	2.727(5)	2.725(5)		O(5)′	112.5(3)	112.1(4)	112.2(1)	112.8(2)	113.2(2)
O(3)–O(5)′	2.700(6)	2.70(1)	2.685(4)	2.685(5)	2.683(5)	O(3)	O(5)′	110.5(2)	110.1(4)	110.3(1)	110.2(2)	110.2(2)
Mean	2.689	2.68	2.672	2.669	2.667			109.5	109.5	109.4	109.4	109.4
			Interlayer K									
K–O(1) × 2	2.846(4)	2.879(7)	2.823(3)	2.896(4)	2.917(4)							
–O(2) × 2	2.879(6)	2.919(9)	2.867(3)	2.942(4)	2.966(5)							
–O(3) × 2	2.850(5)	2.892(8)	2.844(3)	2.910(4)	2.925(4)							
Mean (inner)	2.858	2.897	2.848	2.916	2.936							
K–O(1) × 2	3.301(4)	3.285(6)	3.304(3)	3.285(4)	3.281(4)							
–O(2) × 2	3.507(5)	3.511(9)	3.516(3)	3.486(4)	3.476(5)							
–O(3) × 2	3.287(5)	3.282(8)	3.283(3)	3.269(4)	3.263(5)							
Mean (outer)	3.365	3.359	3.368	3.347	3.340							

TABLE 8. Additional structural details at various temperatures

Parameter	Keystone, South Dakota		Panasqueira, Portugal		
	20°C	300°C	20°C	525°C	650°C
α^*_{tet}(°)	11.3	10.3	11.8	9.8	9.2
β^{**}_{ideal}(°)	94.96	94.97	94.91	94.90	94.90
ψ†(°)					
K site	53.67	53.85	52.90	53.23	53.33
Vac. (oct.)‡	62.24	62.50	62.25	62.26	62.31
Al oct.	57.21	57.23	57.11	57.12	57.15
Sheet thickness (Å)					
Tetrahedral	2.248	2.240	2.234	2.242	2.240
Octahedral	2.097	2.099	2.081	2.090	2.089
Interlayer separation	3.386	3.418	3.436	3.491	3.507
Basal oxygen, Δz_{avg} (Å)	0.209	0.226	0.213	0.210	0.212
Mean vacancy size (Å)	2.243	2.257	2.234	2.245	2.248
Polyhedral-site volumes (Å^3)					
K site	31.40	32.32	30.61	32.92	33.61
Vac. (oct.)	14.27	14.51	14.07	14.29	14.33
Al oct.	9.44	9.48	9.15	9.27	9.29
T(1)	2.28	2.30	2.24	2.24	2.24
T(2)	2.29	2.28	2.25	2.24	2.23
Polyhedral-site bond angle variance,§ σ^2					
K site	7.77	7.28	13.71	10.04	9.34
Vac. (oct.)	108.59	112.14	111.05	111.69	112.89
Al oct.	57.23	60.56	60.46	61.14	62.01
T(1)	4.95	5.20	4.66	5.56	5.06
T(2)	4.76	4.58	3.86	5.29	5.61
Polyhedral-site quadratic elongation,‖ $\langle\lambda\rangle$					
K site	1.002	1.002	1.004	1.003	1.003
Vac. (oct.)	1.036	1.038	1.037	1.038	1.038
Al oct.	1.016	1.017	1.017	1.017	1.017
T(1)	1.001	1.001	1.001	1.001	1.001
T(2)	1.001	1.001	1.001	1.001	1.001

* α_{tet} = (1/2|120° − mean O_b–O_b–O_b angle), where O_b is a basal oxygen.

** $\beta_{ideal} = [180° - \cos^{-1}(a/3c)]$.

† cos ψ = octahedral thickness divided by twice the average M–O,OH, and the ideal value is 54.73°.

‡ The center of the octahedral vacant site is located at 0.7500, 0.2500, 0.000 and is assumed to have no associated estimated standard deviations with these positional parameters.

§ $\sigma^2 = \sum_{i=1}^{n} [\theta_i - \theta_o]^2/(n-1)]$, where θ_o is the ideal bond angle of 90° for an octahedron and 109.47° for a tetrahedron, n is the coordination number, and θ_i is the ith adjacent bond angle from O–M–O or O–T–O angles (see Robinson et al., 1971). For a regular polyhedron, σ^2 is equal to 0.0.

‖ $\langle\lambda\rangle = \sum_{i=1}^{n} [l_i/l_o)^2/n]$, where l_o is the M–O or T–O distance of a regular polyhedron of the same volume, l_i is the M–O_i or T–O_i distance, and n is the coordination number (see Robinson et al., 1971). A regular polyhedron has a $\langle\lambda\rangle$ value of 1.0.

to the K is sufficient to weaken the K–O(2) bond relative to K–O(1) and K–O(3).

The variation of the K–O(2) bond length relative to the other K–O bonds is consistent also with the O(2) atom deviating from the mean basal plane by an out-of-plane tetrahedral corrugation. The corrugations of the basal-oxygen surfaces ($\Delta z = 0.21$ Å) due to the tetrahedral tilting around the vacant M(1) site would produce an irregular interlayer cavity also. It may be noteworthy that the differences between K–O(2) and K–O(1) or K–O(3) increase with elevated temperatures although Δz remains constant. If the K–O(2) bond figures prominantly in the thermal-decomposition mechanism, then the effect should be even more noticeable in paragonite-2M_1 (Lin and Bailey, 1984) where the interlayer cation is smaller. In that structure, the interlayer-cation cavity is more irregular, and the Na–O(2) bond [equal to the Na–O(4) bond of Lin and Bailey] is 2.718 Å as compared to 2.496 and 2.657 Å for the other Na–O bonds. In contrast, trioctahedral micas such as fluorphlogopite do not show an irregular interlayer site both because the corrugation is minimal owing to nearly equal M(1) and M(2) sizes and because the proton orientation more equally affects all K–O bonds.

Figure 3 shows also that the mean interatomic distance of the Al octahedral sites does not vary greatly with temperature and, hence, the octahedral thickness (Table 8) does not expand significantly. Unlike fluorphlogopite, the tetrahedral rotation angle, α, does not approach zero (see Fig. 5). Tetrahedral rotation may be considered an indication of lateral expansion of the octahedral sheet; the rotation angle is a measure of misfit between the two component sheets, and the tetrahedra remain nearly constant in size (within estimated errors) and shape. The change in value of the rotation angle is an indication also of significant movement of the basal-oxygen coordination about the interlayer cation as discussed above. Orientations of the anisotropic atomic vibration, which are not discussed here, are given in Table 9 (see footnote 1).

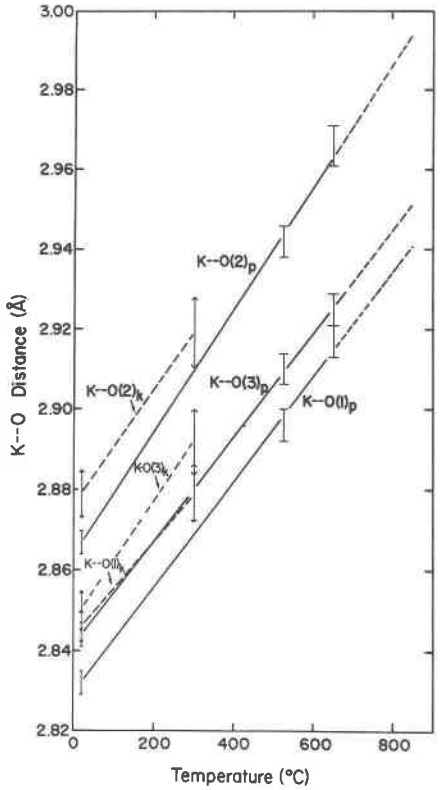

Fig. 4. Interatomic distances for the interlayer site. Symbols and esd as before.

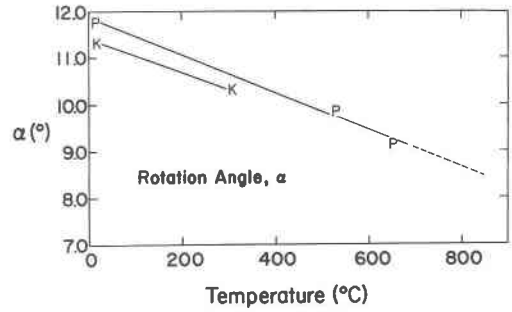

Fig. 5. Tetrahedral rotation angle, α, vs. temperature.

Thermal analysis

The temperatures for dehydroxylation of muscovite as determined by structural analysis (commencing at 850°C) and by thermal analysis (at 475°C) are both based on nonequilibrium conditions and should not be compared. However, the thermal-analysis results of muscovite and pyrophyllite, although not done under precisely identical conditions, are sufficiently similar for the purposes of the discussion. The similarity between the thermal-analysis data of muscovite and pyrophyllite precludes the possibility of assigning the peak at 520°C in pyrophyllite to an interlayer-water-loss event.

Dehydroxylation mechanism

Pauling bond-strength calculations (Pauling's electrostatic valency principle) may be used in a step-wise manner to predict the behavior of muscovite undergoing heat treatment. The structures of muscovite (Rothbauer, 1971) and its dehydroxylate form (Udagawa et al., 1974) are known, and these calculations are simple and straightforward. Similar calculations may be made for muscovite undergoing dehydroxylation if it is assumed that the reaction is not instantaneous (which is implied by the homogeneous concept where all the hydroxyls are indentical and respond to thermal effects in an identical way). Instead, dehydroxylation is considered to be temporal in nature with respect to increasing temperature, where some hydroxyls are lost before others. Although this conclusion may be argued on the basis of kinetics and atom-atom interactions, the thermal-analysis curves clearly indicate that dehydroxylation occurs over a wide temperature interval.

The electrostatic valency principle states that in a stable structure, the total strength of the bonds that reach an anion from all neighboring cations is equal to the formal charge of the anion. For muscovite, Figure 6A and Table 10 show that for any hydroxyl (e.g., J) and any apical oxygen associated with a Si atom (e.g., I), the formal charge of the anion balances the charges received from neighboring cations. For muscovite dehydroxylate (Fig. 6B), Al atoms are in fivefold coordination, and the residual oxygen (e.g., L) is considerably undersaturated with respect to positive charge. In order to compensate, Al atoms coordinated to the residual oxygen (O_r) move closer to it (cf. 1.62 vs. 1.8 Å for the other four Al–O bonds) as shown by arrows at the Al site in Figure 6B and the Al–O_r bond is strengthened considerably (see Udagawa et al., 1974). The undersaturated nature of O_r explains the metastable nature of muscovite dehydroxylate.

Figure 6C shows muscovite in transition between the low-temperature form and the dehydroxylate form. Having fivefold-coordinated sites next to a sixfold-coordinated site produces four apical oxygens (e.g., M) per sixfold site that are oversaturated with respect to positive charge. (In one case out of four, if Al occupies the tetrahedral site, the M oxygen is undersaturated.) In order to compensate for the pattern of oversaturated apical oxygens, the Al ion can move toward the two hydroxyl groups and approximately toward the shared edge (note the range shown by arrows in Fig. 6C) and away from the apical oxygens. In addition, the hydroxyl protons can readjust their positions to polarize further the hydroxyl oxygens. The increased attraction between the Al ion and its coordinating hydroxyl is an effect caused by the neighboring fivefold-coordinated site, and it delays further dehydroxylation until the thermal energy increases sufficiently. This result explains the large temperature interval for dehydroxylation. It is noteworthy that the Al cation is limited in its movement toward the shared edge because of the electrostatic repulsive effects of its Al neighbor.

The anticipated movement of octahedral Al toward the

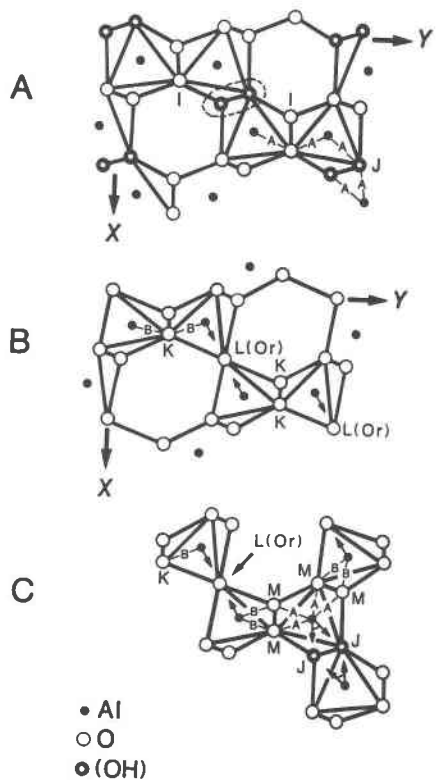

Fig. 6. Al polyhedra for muscovite (A), muscovite dehydroxylate (B), and muscovite in transition (C). Compare the circled portion of (A) to (B). No unit cell is given in (C) because of the lack of periodicity in the proposed transitional structure. Letters refer to either Pauling bond strengths (bonds A and B) or to a specific Pauling bond-strength summation for select oxygens as given in Table 10. The arrows emanating from the Al cation (in B and C) show the direction of movement of this cation.

TABLE 10. Pauling bond-strength calculations for selected bonds and summations for selected oxygen ions

	Pauling bond strengths (PBS) A bonds:0.5 esu B bonds:0.6 esu	
	PBS summation for selected oxygens	
	Muscovite	
I:	Si in tet.: 1.0 + A + A = 2.0 esu	(75%)
	Al in tet.: 0.75 + A + A = 1.75 esu	(25%)
J:	1.0 (proton) + A + A = 2.0 esu	
	Dehydroxylate	
K:	Si in tet.: 1.0 + B + B = 2.2 esu	(75%)
	Al in tet.: 0.75 + B + B = 1.95 esu	(25%)
L:	B + B = 1.2 esu	
	In transition (J, K, L)	
M:	Si in tet.: 1.0 + A + B = 2.1 esu	(75%)
	Al in tet.: 0.75 + A + B = 1.85 esu	(25%)

Note: Refer to Fig. 6. Summations J, K, and L are appropriate for muscovite in transition also.

remaining OH groups effectively oversaturates the oxygen of each OH group, which was electrostatically neutral prior to this re-adjustment. The consequence of this oversaturation is to weaken (lengthen) slightly the O–H bond. This weakening of the O–H bond explains the downward shift in frequency as observed in IR spectra by Gaines and Vedder (1964) and Aines and Rossman (1985) for the band at 3628 cm^{-1}, which shifts toward 3600 cm^{-1} upon dehydroxylation. The slight weakening of the O–H bond does not produce an immediate dehydration event, suggesting that the Al–OH bond may be equally or more important to the dehydroxylation process than is the O–H bond.

Figure 6C shows a pair of Al–O,OH polyhedra with all neighboring Al–O polyhedra in fivefold coordination. Clearly, however, Al–O,OH polyhedra pairs may be linked to either ^{v}Al–O or ^{vi}Al–O,OH polyhedra. For one extreme, where all neighboring polyhedra are ^{vi}Al–O,OH, hydroxyl loss is relatively easy, whereas for the other extreme, where all neighboring polyhedra are ^{v}Al–O, hydroxyl loss is more difficult. Thus, a bimodal distribution is anticipated as is observed in the thermal-analysis curves. Distributions are possible, however, that include both ^{v}Al and ^{vi}Al neighbors, and such distributions produce the observed broadening of the thermal peaks.

This model is compatible with all observed data. In addition, the model is sufficiently general to be applied to other dioctahedral 2:1 layer silicates, including pyrophyllite. In regard to the latter, the model explains the specific nature of the NMR Si-resonance peak for the sample treated at 565°C in MacKenzie et al. (1985). In addition to any general loss in crystallinity caused by heating, the large number of different Al–O bond lengths due to the distortional effects of neighboring Al polyhedra results in the marked decrease in apparent peak area and produces very broad spectral lines that blend into the background in the ^{27}Al NMR spectra. [Both MacKenzie et al. (1985) and Frost and Barron (1984) suggested that the spectra are strongly influenced by changes in the symmetry around the Al.] Therefore, the small peaks near chemical shifts of 60 and 70 ppm represent a significant dehydroxylate contribution. Hence, the model suggests that ^{27}Al NMR spectra taken while pyrophyllite is in transition should not correlate well to models involving Al–O bond lengths derived by simply adding components of pyrophyllite and pyrophyllite dehydroxylate structures.

It is interesting to note that rehydroxylation may take place in muscovite and pyrophyllite forms if the dehydroxylation reaction is not complete (Gaines and Vedder, 1964, etc.). Although the Al–O_r bond is strong in the dehydroxylate structure, the stability of the dehydroxylate structure relative to the fully hydrated form is lower. (Similarly, because there are fewer residual oxygens in the transitional forms, the stability of these forms is greater than that of the dehydroxylate also.) Because the H can merely rebond itself to the residual oxygen, the Al–O_r bond is not broken upon rehydroxylation, although the

oxygen configuration about the Al is changed considerably. Apparently, rehydroxylation is more likely if the fivefold sites are distorted also, as they are in transition between the low-temperature and high-temperature forms (note that the oxygens labeled M in Fig. 6C belong to the fivefold Al sites also).

The model as presented here should be applicable to all dioctrahedral 2:1 layer silicates except perhaps the brittle micas. In muscovite, the K–O(2) bond must be broken during dehydroxylation, whereas in pyrophyllite no such bond exists. Therefore, the temperature of dehydroxylation and possibly the size of the thermal peaks should be dependent partially on the number of interlayer sites occupied and the type of the interlayer cation. Work is in preparation to expand the model to include interlayer-cation chemistry and occupancy.

Conclusions

Dehydroxylation occurs at temperatures where the silicate ring is ditrigonal. Therefore, possible misfit between the dioctahedral-tetrahedral sheet interface is not an important consideration in the thermal-decomposition mechanism of muscovite. The proton is located in muscovite in a position to weaken the K–O(2) bond, thereby providing a path of migration upon dehydroxylation. The model for the dehydroxylation process as presented here does not conform to either the homogeneous or inhomogeneous process as presented by Taylor (1962) and supports the work by Heller-Kallai and Rozenson (1980). It is proposed that after dehydroxylation is initiated, neighboring coordination polyhedra are affected, and the remaining hydroxyl groups become more strongly bonded to the Al cations. Muscovite in transition is not simply a combination of the low-temperature and high-temperature structural forms. Pauling's electrostatic valency principle may be used to show that the anion framework requires a readjustment of bond lengths and angles around the Al cations during the transition. Hence, there are many different transitional forms as dehydroxylation proceeds. A bimodal distribution of dehydroxylation around two extremes occurs with the hydroxyl group being lost at lower temperatures where neighboring polyhedra are in octahedral coordination and at higher temperatures where neighboring polyhedra are in fivefold coordination.

In contrast to previous studies, it is attempted here to understand dehydroxylation while it occurs, which is fundamentally a process-oriented approach. The strengths of this approach are that it uses static configurations and dynamic changes and that it is not just a description of a static crystal structure at a specified temperature. Dynamic changes are difficult to determine experimentally, but by using Pauling's rules, it is still possible to understand atomistically the process of dehydroxylation. It should be recognized that such a process involves dynamic aspects influenced by kinetics, all of which may be delineated by this approach. Equally important is the realization that, as a process, it is applicable to both nonequilibrium and equilibrium reactions.

Acknowledgments

We thank E. Glover of the University of Wisconsin–Madison and G. Harris of the University of Illinois at Chicago for the chemical analyses and P. van Kriekan, Instituut voor Aardwetenschappen of the University of Utrecht, for the thermal analysis. Jing Han assisted in the Panasqueira muscovite data collection, and Stephen Bouchard calibrated the furnace for those data collection. The manuscript benefited from reviews by M. Lipsicas, H. S. Yoder, Jr., and R. M. Hazen. Portions of this work were supported by National Science Foundation Grant EAR80-18222 and Petroleum Research Foundation of the American Chemical Society Grant 17263-AC2.

References

Aines, R.D., and Rossman, G. R. (1985) The high temperature behavior of trace hydrous components in silicate minerals. American Mineralogist, 70, 1169–1179.

Brown, G.E., Sueno, S., and Prewitt, C.T. (1973) A new single-crystal heater for the precession camera and four-circle diffractometer. American Mineralogist, 58, 698–704.

Busing, W.R., Martin, K.O., and Levy, H.A. (1962) ORFLS, a Fortran crystallographic least-squares refinement program. U.S. National Technical Information Service, ORNL-TM-305.

——— (1964) ORFFE, a Fortran crystallographic function and error program. U.S. National Technical Information Service, ORNL-TM-306.

Cromer, D.T., and Mann, J.B. (1968) X-ray scattering factors computed from numerical Hartree-Fock wave functions. Acta Crystallographica, A24, 321–324.

Freund, F. (1970) Infrared spectra of $Mg(OH)_2$ at elevated temperatures. Spectrochemica Acta, 26A, 195–205.

Frost, R.L., and Barron, P.F. (1984) Solid-state silicon-29 and aluminum-27 nuclear magnetic resonance investigation of the dehydroxylation of pyrophyllite. Journal of Physical Chemistry, 88, 6206–6209.

Gaines, G.L., Jr., and Vedder, W. (1964) Dehydroxylation of muscovite. Nature, 201, 495.

Grim, R.E. (1968) Clay mineralogy. McGraw-Hill, New York.

Grim, R.E., Bradley, W.F., and Brown, G. (1951) X-ray identification and crystal structures of clay minerals, G.W. Brindley, Ed., Mineralogical Society, London, p. 138–172.

Hazen, R.M. (1977) Temperature, pressure and composition: Structurally analogous variables. Physics and Chemistry of Minerals, 1, 83–94.

Hazen, R.M., and Finger, L.W. (1982) Comparative crystal chemistry. Wiley, New York, 231 p.

Heller-Kallai, L., and Rozenson, I. (1980) Dehydroxylation of dioctahedral phyllosilicates. Clays and Clay Minerals, 28, 355–368.

Koster van Groos, A.F., and Guggenheim, S. (1984) The effect of pressure on the dehydration reaction of interlayer water in Na montmorillonite (SWy-1). American Mineralogist, 69, 872–879.

——— (1986) The dehydration of K-exchanged montmorillonite at elevated temperatures and pressures. Clays and Clay Minerals, 34, 281–286.

——— (1987) The dehydration of a Ca- and Mg-exchanged montmorillonite (SWy-1) at elevated pressures. American Mineralogist, 72, 292–298.

Lee, J.H., and Guggenheim, S. (1981) Single crystal X-ray refinement of pyrophyllite-1Tc. American Mineralogist, 66, 350–357.

Lenhart, P.G. (1975) An adaptable disk-oriented automatic diffractometer control system. Journal of Applied Crystallography, 8, 568–570.

Lin, C-Y., and Bailey, S.W. (1984) The crystal structure of paragonite-$2M_1$. American Mineralogist, 69, 122–127.

MacKenzie, R.C., and Milne, A.A. (1953) Effect of grinding on muscovite. Mineral Magazine, 30, 178–185.

MacKenzie, K.J.D., Brown, I.W.M., Meinhold, R.H., and Bowden, M.E. (1985) Thermal reactions of pyrophyllite studied by high-resolution solid state ^{27}Al and ^{29}Si nuclear magnetic resonance spectroscopy. American Ceramic Society Journal, 68, 266–272.

North, A.C.T., Phillips, D.C., and Mathews, F. (1968) A semi-empirical method of absorption correction. Acta Crystallographica, A24, 351–359.

Rothbauer, R. (1971) Untersuchung eines $2M_1$-Muskovits mit Neutronenstrahlen. Neues Jahrbuch für Mineralogie Monatshefte, 143–154.

Symmes, G.H. (1986) The thermal expansion of natural muscovite, paragonite, margarite, pyrophyllite, phlogopite, and two chlorites: The significance of high T/P volume studies on calculated phase equilibria. B.A. Thesis, Amherst College, Amherst, Massachusetts.

Takeda, H., and Morosin, B. (1975) Comparison of observed and predicted structural parameters of mica at high temperatures. Acta Crystallographica, B31, 2444–2452.

Takeda, H., Haga, N., and Sadanaga, R. (1971) Structural investigation of polymorphic transition between $2M_2$-, 1M-lepidolite and $2M_1$-muscovite. Mineralogical Journal (Japan), 6, 203–215.

Taylor, H.F.W. (1962) Homogeneous and inhomogeneous mechanisms in the dehydroxylation of minerals. Clay Minerals Bulletin, 5, 45–55.

Toraya, H. (1981) Distortions of octahedra and octahedral sheets in 1M micas and the relation to their stability. Zeitschrift für Kristallographica, 157, 173–190.

Udagawa, S., Urabe, K., and Hasu, H. (1974) The crystal structure of muscovite dehydroxylate. Japanese Association of Mineralogists, Petrologists, and Economic Geologists, 69, 381–389.

Vaughan, M.T., and Guggenheim, S. (1986) Elasticity of muscovite and its relationship to crystal structure. Journal of Geophysical Research, 91, 4657–4665.

Vedder, W., and Wilkins, R.W.T. (1969) Dehydroxylation and rehydroxylation, oxidation and reduction of micas. American Mineralogist, 54, 482–509.

Wardle, R., and Brindley, G.W. (1972) The crystal structures of pyrophyllite-1Tc and of its dehydroxylate. American Mineralogist, 57, 732–750.

Wirth, R. (1985) Dehydration of mica (phengite) by electron bombardment in a transmission electron microscope (TEM). Journal of Material Science Letters, 4, 327–330.

Yoder, H.S., and Eugster, H.P. (1955) Synthetic and natural muscovites. Geochimica et Cosmochimica Acta, 8, 225–280.

Manuscript received October 7, 1986
Manuscript accepted February 13, 1987